A Simple Method to Reduce Torque Ripple in Direct Torque Controlled Permanent Magnet Synchronous Motor by Using Voltage Vectors with Variable Amplitude and Position

Yongchang Zhang*, Jianguo Zhu, Senior Member, IEEE, Wei Xu, Member, IEEE, Youguang Guo, Senior Member, IEEE

Abstract—In this paper, a modified direct torque control (DTC) for permanent magnet synchronous machine is proposed, which enables important torque and flux ripple reduction by using voltage vectors with variable amplitude and angle. Conventional DTC presents some drawbacks, including large torque ripple, variable switching frequency and acoustic noise. The reason lies in that the switching table is composed of a limited number of discrete voltage vectors with fixed amplitude and position. Moreover, the selected vector will work during the whole sampling period, and hence their effects on torque and flux may usually be too large or too small. In the proposed DTC, the amplitudes of torque and flux errors are differentiated and they are employed to regulate the amplitude and position of the output voltage vectors on-line, which would finally be synthesized by space vector modulation (SVM). Two simple formulas are developed to derive the amplitude and position of the commanding voltage vectors from the errors of torque and flux. Conventional switching table and hysteresis controllers are eliminated and fixed switching frequency is obtained with the help of SVM. Stator flux is estimated from an improved voltage model, which is based on a low-pass filter with compensations of the amplitude and phase. The proposed DTC exhibits excellent dynamic performance and significant torque ripple reduction at steady state, which are validated by the presented simulation and experimental results.

Index Terms—Torque control, AC motor drives, permanent magnet synchronous motor, space vector modulation, low-pass filters

Nomenclature

$\alpha\beta$	Stationary stator reference frame axes
$\psi_\mathbf{r}$	Rotor flux vector in stationary coordinate
$\psi_\mathbf{s}$	Stator flux vector in stationary coordinate
$\mathbf{i}_\mathbf{s}$	Stator current vector in stationary coordinate
$\mathbf{u}_\mathbf{s}$	Stator voltage vector in stationary coordinate
δ	Electrical angle between stator flux vector and rotor flux vector
ω	Rotor speed
ψ_d, ψ_q	d-axis and q-axis stator flux
ψ_f	Permanent magnet flux
θ_r	Rotor angle
dq	Rotary rotor reference frame axes
i_d, i_q	d-axis and q-axis stator current
L_d, L_q	d-axis and q-axis inductance
L_s	Synchronous inductance
p	Number of pole pairs
R_s	Stator resistance
T_e	Electromagnetic torque

u_d, u_q d-axis and q-axis stator voltage

I. INTRODUCTION

Permanent magnet synchronous machines (PMSM) are receiving wide attention for industry applications due to their high efficiency, high power/torque density and high reliability [1]–[3]. For the applications requiring high dynamic performance, current vector control (CVC) is often employed [4], [5]. Recently another high performance control technique, named direct torque control (DTC), which was initially developed for induction motor (IM) drives [6]–[8], has also been investigated in PMSM drives [3], [9]–[11]. Compared to CVC, DTC directly manipulates the final output voltage vector without the need of inner current loops, and hence eliminates the inherent delay caused by current loops and features a high dynamic response. All calculations are implemented in stationary coordinate, so the structure of DTC is simple. Moreover, DTC only needs the stator resistance to estimate the stator flux, so it is less affected by the motor parameter variations.

Despite the merits above, DTC also presents some drawbacks, including large torque ripple, variable switching frequency along with acoustic noises, among others [8], [12], [13]. This is because DTC is a kind of heuristic method in essence, which uses hysteresis comparators and stator flux position information to determine the final output voltage vector from a switching table. The hysteresis comparators only consider the signs of torque and flux errors, and do not differentiate their amplitudes. Furthermore, the switching table is composed of a limited number of discrete voltage vectors with fixed length and position. If a vector is selected, it will work during the whole sampling period, which may regulate the torque and flux too much or too less. Because of the reasons above, although good dynamic performance and strong robustness are achieved in classical DTC, it also brings a variable switching frequency and large torque ripple.

To overcome the drawbacks of the classical DTC, many methods have been proposed in the literature [2]–[4], [11], [13]–[22]. These methods can be divided into various categories based on different philosophy or views. As DTC motor drives are mostly fed by voltage source inverters (VSI), where voltage vectors are the final output variables, it is possible to

obtain improved performance by adjusting the intensity of the voltage vector moderately. There are two properties for the voltage vectors, i.e. amplitude and position, so the effect of voltage vector can be regulated from these two aspects.

Some authors changes the vector length by adjusting the duty ratio of the active vector, i.e. one or two active vectors and one null vector are applied during one sampling period [21], [23]–[25]. The active vector is obtained from the conventional switching table, and the duty ratio is determined according to various principles, including torque ripple minimization [23], [25], [26], fuzzy logic adaptation [24], equalizing the mean torque with the reference value over one cycle [21], etc. These methods are complicated and usually require the knowledge of motor parameters and rotor speed, which negates the merits of classical DTC.

Other authors [27] paid more attention to the angle of voltage vector by selecting the voltage vector located within a certain area. Two methods for obtaining the voltage vector angle were proposed in [27]. The first method employs torque and flux errors to acquire the voltage angle, while the second relies much on the knowledge of motor parameters, hence decreasing the robustness and simplicity. Furthermore, in both methods, only angle of the voltage vector is considered and the amplitude is kept constant, so the performance improvement is limited.

Space vector modulation (SVM) can produce arbitrary voltage vector with any amplitude and angle within the linear range, so it has been widely adopted in DTC to regulate the torque and flux more moderately and accurately [3], [8], [10], [11], [17], [27]–[32]. Another advantage of employing SVM is that fixed switching frequency can be obtained. A multitude of schemes were developed to obtain the commanding voltage vector, including deadbeat control [17], indirect torque control [19] or variations [32], stator flux oriented control or the like [3], [8], [11], [28]–[30], etc. Different torque and flux controllers are incorporated in the system to produce the desired d-axis and q-axis voltage component, including proportional integral (PI) controller [29], sliding mode controller [10], and so on. The SVM-based DTC provides low torque ripple and fixed switching frequency. The main drawback is that most of them require rotary coordinate transformation, much knowledge of motor parameters and high computational ability, so the robustness and simplicity of conventional DTC are sacrificed.

To eliminate the parameter dependence, some authors suggested using discrete SVM [8], [22]. A more accurate and complex switching table is constructed by dividing one sampling period into two or three intervals, using more levels in the hysteresis comparators and taking rotor speed into account. This method leads to reduced torque ripple, but at the cost of complexity in switching table, especially when the number of intervals increases. Another method to obtain increased number of voltage vectors is to use multilevel inverter [13], [18], [33], which increases the hardware cost and system complexity, because other problems concerning circuit topology limitation, e.g. neutral point balance for three-level inverter DTC [13], should be addressed. Recently discrete SVM has been extended to three-level inverter DTC [18].

It can solve the problems such as neutral point balance at the pulsewidth modulation level, hence decoupling the performance improvement of DTC from the circuit limitation. However, the voltage vector amplitude is constant in [18], so the torque ripple reduction is not obvious.

Recently model predictive control (MPC) was introduced to achieve high dynamic torque control [15], [16], [34]. It is similar to DTC only in that they both directly select one and only one voltage vector. However, their principles are very different. DTC uses a heuristic switching table to obtain the output vector quickly, while MPC defines a cost function to evaluate the effects of every possible voltage vector and the one minimizing the cost function is selected. Although it can achieve better performance, MPC requires more intensive computation and relies heavily on the accuracy of system model and parameters [34].

In this paper, an improved DTC is proposed, which eliminates the use of hysteresis comparators and switching table. It makes full use of the ability of SVM to produce arbitrary voltage vector. Different from the existing methods, both the amplitude and angle of voltage vector are considered and they are devised from the torque and flux errors only, so the improved DTC features a simple structure and maintains the parameter robustness of conventional DTC. The position of stator flux is still needed in the proposed DTC. A low-pass filter (LPF) based estimator with compensations of amplitude and angle is employed to obtain this information. The LPF based voltage model requires stator resistance only and has been successfully applied in the stator flux oriented control [35]. Simulation and experimental results are given in this paper to confirm the effectiveness of the proposed schemes.

II. MODEL OF PMSM

A. Machine Equations

The dynamic model of a PMSM machine in the rotor synchronous dq coordinate can be expressed as

$$\begin{bmatrix} u_d \\ u_q \end{bmatrix} = R_s \begin{bmatrix} i_d \\ i_q \end{bmatrix} + \begin{bmatrix} pi_d & -\omega L_q \\ \omega L_d & pi_q \end{bmatrix} \begin{bmatrix} i_d \\ i_q \end{bmatrix} + \begin{bmatrix} 0 \\ \omega \psi_f \end{bmatrix} \quad (1)$$

and the stator flux equations are

$$\begin{bmatrix} \psi_d \\ \psi_q \end{bmatrix} = \begin{bmatrix} L_d & 0 \\ 0 & L_q \end{bmatrix} \begin{bmatrix} i_d \\ i_q \end{bmatrix} + \begin{bmatrix} \psi_f \\ 0 \end{bmatrix} \quad (2)$$

The electromagnetic torque is expressed as

$$T_e = \frac{3}{2} p (\psi_d i_q - \psi_q i_d) = \frac{3}{2} p [\psi_f i_q + (L_d - L_q) i_d i_q] \quad (3)$$

$$= \frac{3p |\psi_s|}{4 L_d L_q} [2\psi_f L_q \sin \delta + |\psi_s| (L_d - L_q) \sin 2\delta] \quad (4)$$

and it is composed of two parts: the permanent magnet torque and the reluctance torque caused by the rotor saliency.

For surface-mounted PMSM (SPMSM) without saliency, the d-axis and q-axis inductance are equal to synchronous inductance, i.e. $L_d = L_q = L_s$. The torque does not include the reluctance torque and is simplified as

$$T_e = \frac{3}{2} p \psi_f i_q = \frac{3}{2} p \frac{\psi_f |\psi_s|}{L_s} \sin \delta \quad (5)$$

and the voltage equations and stator flux equations are also simplified. They can be expressed in stationary frame (the components indicated by $\alpha\beta$) using complex vector as

$$\mathbf{u_s} = \mathbf{R_s}\mathbf{i_s} + p\psi_s \qquad (6)$$
$$\psi_s = \mathbf{L_s}\mathbf{i_s} + \psi_r \qquad (7)$$

where $\psi_r = \psi_f e^{j\theta_r}$ and the torque in stationary frame is expressed as

$$T_e = \frac{3}{2}p\psi_s \otimes \mathbf{i_s} = \frac{3}{2}p(\psi_{s\alpha}i_{s\beta} - \psi_{s\beta}i_{s\alpha}) \qquad (8)$$

B. Effects of Voltage Vectors on Torque

From (5), it is found that the torque T_e can be changed quickly by adjusting the angle δ [9]. This is the basic principle of conventional DTC. The differentiation of T_e with respect to time t is

$$\frac{dT_e}{dt} = \frac{dT_e}{d\delta}\frac{d\delta}{dt} = \frac{3}{2}p\frac{\psi_f|\psi_s|}{L_s}\cos\delta\frac{d\delta}{dt} \qquad (9)$$

For VSI-fed DTC, the voltage vector is the sole controllable input variable, so the change of angle δ can be only achieved through the effects of voltage vectors. From (6), if neglecting the stator resistance voltage drop, it is seen that the stator flux ψ_s can be changed quickly by changing the applied voltage vector, and then δ changes, resulting in fast torque response. However, the relationship between δ and $\mathbf{u_s}$ is complicated, so the analysis above is just a crude heuristic analysis and it is desirable to obtain the direct relationship between T_e and $\mathbf{u_s}$.

From (6) and (7), we can get

$$L_s\frac{d\mathbf{i_s}}{dt} = \mathbf{u_s} - R_s\mathbf{i_s} - j\omega\psi_r \qquad (10)$$

From (8), the torque differentiation with respect to time t is

$$\frac{dT_e}{dt} = \frac{3}{2}p\left[\frac{d\psi_s}{dt}\otimes\mathbf{i_s} + \frac{d\mathbf{i_s}}{dt}\otimes\psi_s\right] \qquad (11)$$

Substitute (6), (7) and (10) into (11) and omit the tedious derivation process, the final torque differentiation is

$$L_s\frac{dT_e}{dt} = -R_sT_e - \frac{3}{2}p\omega\psi_r\cdot\psi_s + \frac{3}{2}p\psi_r\otimes\mathbf{u_s}$$
$$= \Delta T_{e1} + \Delta T_{e2} + \Delta T_{e3} \qquad (12)$$

It is seen from (12) that the torque differentiation is composed of three parts, just similar to the case in induction motor [23]. The first part ΔT_{e1} is always negative with respect to T_e; the second part ΔT_{e2} is also negative and proportional to rotor speed; the last term ΔT_{e3} is positive and it reflects the effect of stator voltage on T_e. ΔT_{e3} tells that the cross product of $\mathbf{u_s}$ and ψ_r determines the rising slope of torque. Because ψ_r is a rotating vector with constant amplitude of PM flux, the effects of ΔT_{e3} can be regulated by changing the intensity of $\mathbf{u_s}$, which is achieved by adjusting the amplitude and position.

In this paper, both the amplitude and position of the voltage vectors will be regulated, so better performance is expected

[21], [23], [24] only. Because only the knowledge of torque and flux errors is required, the dependence on motor model and parameters is eliminated, as introduced in Section III.

III. PROPOSED DTC SCHEME

A. Voltage Vector Angle Determination

In conventional DTC, if the stator flux vector is located within a certain area, such as $\pm30°$, a fixed vector (V_2, V_3, V_5 or V_6), depending on the sign of torque and flux errors, will be selected regardless of the amplitudes of errors, as illustrated in Fig. 1. This achieves good robustness, but fails to regulate torque and flux accurately and moderately. To achieve better performance, the angle of voltage vector should be determined according to the torque and flux errors and stator flux position, as illustrated in Fig. 2.
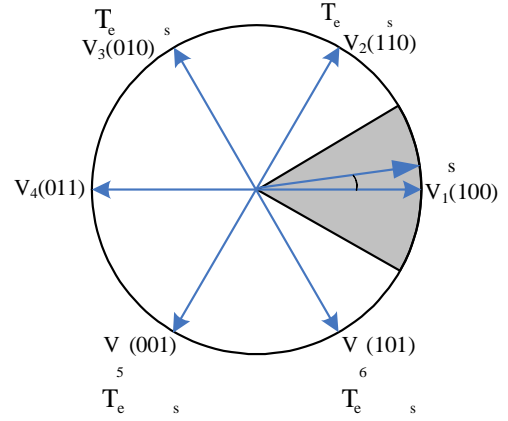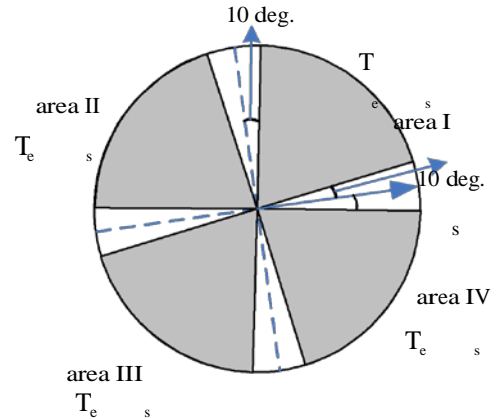

Fig. 1. Vector selection in conventional DTC

Fig. 2. Vector selection in proposed DTC

than those changing vector position [18], [27] or amplitude

If the stator flux angle φ is known and the toque and flux should increase, the candidate vector can be selected from the shaded area I within the range of $(\varphi + 10°, \varphi + 80°)$. The area within $(\varphi, \varphi + 10°)$ and $(\varphi + 80°, \varphi + 90°)$ are not considered to avoid sharp change in flux and torque. When the torque error is large or small, the vector near $\varphi + 80°$ or $\varphi + 10°$ should be selected, which considers the amplitude

of torque error. From the view of torque regulation, the angle increment of voltage vector with respect to stator flux position is expressed as

$$\Delta\varphi_T = \frac{E_T}{C_T} \cdot \frac{\pi}{2} = \frac{T_e^* - T_e}{C_T} \cdot \frac{\pi}{2} \qquad (13)$$

where T_e^* is the reference values for torque and C_T is a positive constant. For the purpose of stator flux regulation, the angle increment of voltage vector should be negatively proportional to the stator flux change, i.e.

$$\Delta\varphi_\psi = \left(1 - \frac{E_\psi}{C_\psi}\right) \cdot \frac{\pi}{2} = \left(1 - \frac{\psi_s^* - \psi_s}{C_\psi}\right) \cdot \frac{\pi}{2} \qquad (14)$$

where ψ_s^* is the reference values for torque and C_ψ is a posi- tive constant. (13) and (14) reflect the influences of amplitudes of torque error and flux error on the angle increment of voltage

vector, which are not considered in conventional DTC. In practical application, the torque change should be considered preferably, so different weight factors are imposed to (13) and (14). The final angle increment of voltage vector with respect to stator flux is

$$\Delta\varphi = \begin{cases} k\Delta\varphi_T + (1-k)\Delta\varphi_\psi & \text{area I} \\ k(\pi - \Delta\varphi_T) + (1-k)(\pi - \Delta\varphi_\psi) & \text{area II} \\ -k\Delta\varphi_T - (1-k)\Delta\varphi_\psi & \text{area III} \\ k(-\pi + \Delta\varphi_T) + (1-k)(-\pi + \Delta\varphi_\psi) & \text{area IV} \end{cases} \qquad (15)$$

where k is a positive constant and it is usually chosen larger than 0.5 to give torque change more weighting factor.

B. Voltage Vector Amplitude Determination

The influences of voltage vector on torque and flux are not only decided by the angle, but also by the amplitude, as shown in (12). The length of applied voltage vector can be regulated by adjusting its time duration during one sampling period, which is also defined as duty ratio [24], and the rest of time is allocated for a null vector. In the previous literature [21], [23]–[26], the working time or duty ratio of the nonzero vector was obtained through analytical methods, requiring complicated calculation and accurate motor parameters, which negates the merits of DTC. In this paper, a very simple method to obtain the duty ratio or equivalent voltage vector length is proposed, which is expressed as

$$m = \frac{E_T}{C_T} + \frac{E_\psi}{C_\psi} = \frac{T_e^* - T_e}{C_T} + \frac{\psi_s^* - \psi_s}{C_\psi} \qquad (16)$$

m is normalized with respect to maximum peak value of phase voltage in the linear range, i.e. $U_{dc}/\sqrt{3}$, where U_{dc} is the dc bus voltage. In practical use, rated torque and stator flux provide a quick reference for C_T and C_ψ, which can be easily obtained from the nameplate of machine.

Based on (15) and (16), the final output voltage vector is expressed as

$$V = m \cdot e^{j(\varphi + \Delta\varphi)} \qquad (17)$$

IV. STATOR FLUX ESTIMATION

Accurate stator flux estimation is mandatory for the stator flux loop control and the synthesis of commanding voltage vector in (17). There are two kinds of models to estimate the stator flux: voltage model and current model. The voltage model shown in (6) is preferred because it only requires the stator resistance while the current model (7) requires the knowledge of rotor position and d-axis and q-axis inductance. Directly integrating the back electromotive force (EMF) is not practicable in digital implementation, because it suffers from the problems of dc drift and initial value. To eliminate the dc

component, a high-pass filter (HFP) should be incorporated. A pure integrator in series with a HPF is equivalent to a filter LPF and there are steady state errors in magnitude and phase, so appropriate compensation is necessary to enhance the steady performance. The steady errors in the amplitude and phase of LPF with respect to ideal integrator are

$$\Delta\theta = \arctan\frac{\omega_e}{\omega_c} - \frac{\pi}{2} = -\arctan\frac{\omega_c}{\omega_e} \qquad (18)$$

$$\Delta G = \frac{\frac{\omega_e}{\sqrt{\omega_e^2 + \omega_c^2}}}{\omega_e} \qquad (19)$$

where ω_e is the synchronous frequency of stator flux and ω_c is the cut-off frequency of LPF. Knowing the steady errors, the corresponding compensation is designed as

$$G = \Delta G \times e^{\Delta\theta} = \frac{\frac{\omega_e}{\sqrt{\omega_e^2 + \omega_c^2}}}{\omega_e} e^{-\arctan\frac{\omega_c}{\omega_e}} = 1 + \frac{\omega_c}{j\omega_e} \qquad (20)$$

In conventional LPF, fixed cut-off frequency is employed and the performance will degrade when the stator frequency is lower than the cut-off frequency, especially at low speeds. Very low cut-off frequency can mitigate this problem, but the effectiveness of eliminating dc component is degraded. To improve the performance, the cut-off frequency should vary with the stator frequency, i.e. $\omega_c = k\omega_e$, where k is usually chosen between 0.1 and 0.5. The synchronous frequency ω_e can be calculated from stator flux as

$$\omega_e = \frac{\psi_s \otimes p\psi_s}{\|\psi_s\|^2} = \frac{\psi_\alpha(u_\beta - R_s i_\beta) - \psi_\beta(u_\alpha - R_s i_\alpha)}{\psi_\alpha^2 + \psi_\beta^2} \qquad (21)$$

The whole diagram of LPF with compensation is illustrated in Fig. 3. Fig. 4 shows the simulation results of real and estimated stator flux when the PMSM starts from standstill to 1000 rpm using the proposed DTC. It is seen that the estimated flux converges to the real flux quickly and they are exactly matched in the steady state.

and it is synthesized by SVM.

V. Experimental Results

The proposed DTC was experimentally tested in a two-level inverter-fed PMSM motor drive. The structure of the whole system is illustrated in Fig. 5. A dSpace DS1104 PPC/DSP control board is employed to implement the real-time algorithm coding using C language. A three-phase intelligent power module equipped with IGBTs is used for an inverter. The gating pulses are generated in the DS1104 board and then
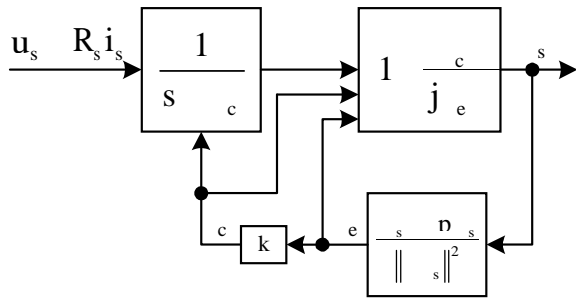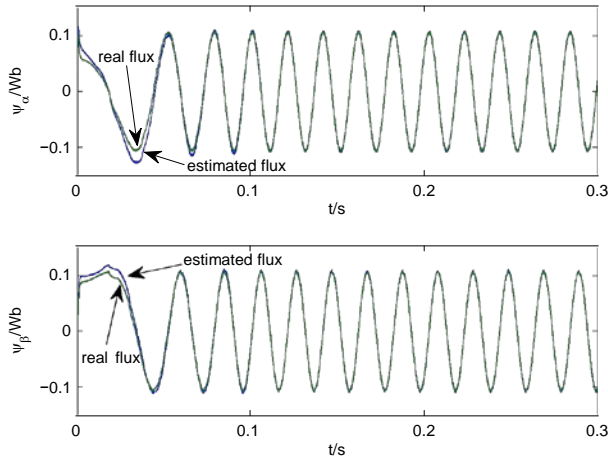
Fig. 3. LPF with compensation

Fig. 4. Stator estimation using LPF with compensation (simulation)

TABLE I
MOTOR AND SYSTEM PARAMETERS

Rated power	P_N	1kW
Number of pole pairs	p	3
Permanent magnet flux	ψ_f	0.1057 Wb
Stator resistance	R_s	1.8Ω
d-axis and q-axis inductance	L_d, L_q	15 mH
Rated speed	n_N	2000 rpm
Rated torque	T_N	4.8 Nm
Rated line-line voltage	U_N	128 V
Sampling period	T_s	100 µs
Speed loop sampling period	T_{speed}	1000 µs
Torque constant gain	C_T	2 Nm
Flux constant gain	C_ψ	0.1 Wb
Stator flux reference	ψ_s^*	0.12 Wb

Firstly, the steady-state responses at low and high speeds are investigated. Fig. 6, Fig. 7 and Fig. 8 present the steady low speed response at 200 rpm without load for classical DTC, DTC1 and DTC2, respectively. From top to bottom, the curves are stator flux and electromagnetic torque. The responses at high speed of 2000 rpm for the three kinds of DTC are illustrated in Fig. 9, Fig. 10 and Fig. 11, respectively. It is seen that in both DTC1 and DTC2, the torque ripples are reduced significantly compared to that in the classical DTC. The torque ripple reduction is even higher for DTC2, validating the effectiveness of regulating both vector angle and amplitude. For DTC1 with fixed amplitude of vectors, the torque ripple reduction increases with the speed, while the flux ripple is comparable to that in classical DTC, and a slight flux ripple reduction is exhibited at high speed.
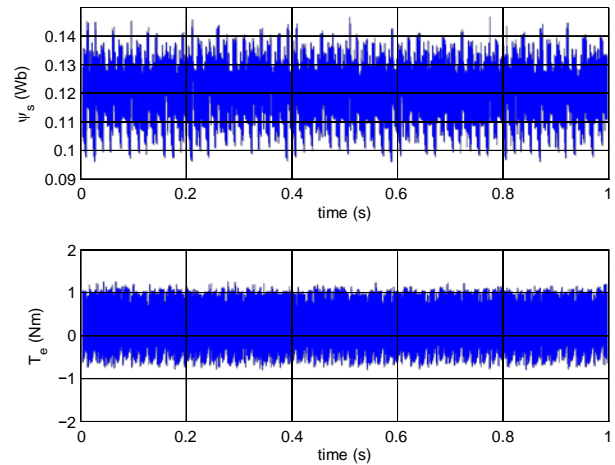
sent to the inverter. The load is applied using a programmable dynamometer controller DSP6000. A 2500-pulse incremental encoder is equipped to obtain the rotor speed of PMSM. All experimental results are recorded using the ControlDesk interfaced with DS1104 and PC. The parameters of motor and control system are listed in Tab. I. Extensive experimental tests were carried out to compare the performances of the improved DTC with that of classical DTC, including steady-state response at low speed and high speed, start-up response and response to external load disturbance. The classical DTC, improved DTC regulating the vector angle only and regulating both vector angle and amplitude, are referred as "classical", "DTC1" and "DTC2", respectively, as illustrated in the following experimental results. The constant vector length in DTC1 is $m = 0.98$.

Fig. 6. Steady state response at 200 rpm for classical DTC

Fig. 5. Block diagram of proposed DTC

To further test the superiority of DTC2 over DTC1, Fig. 12 shows the torque and flux waveforms when switching from DTC1 to DTC2 at 500 rpm without load. It is seen that the ripples in both torque and stator flux are reduced significantly, validating the effectiveness of regulating voltage amplitude.
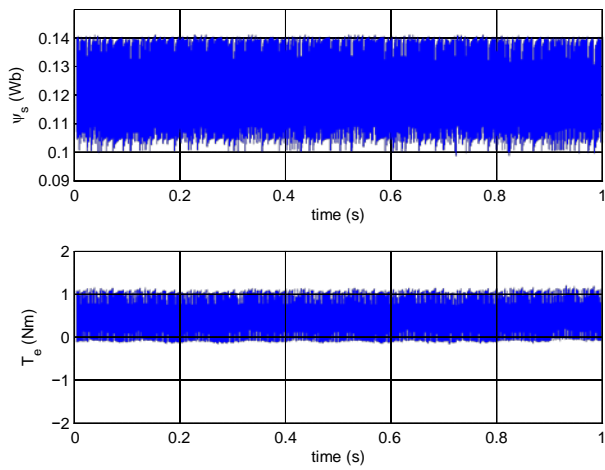
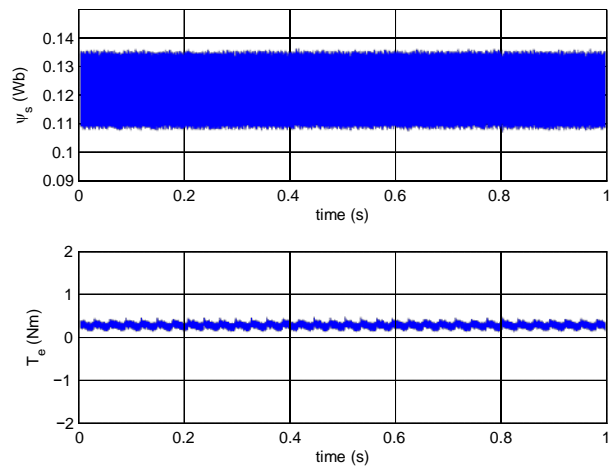Fig. 7.   Steady state response at 200 rpm for DTC1

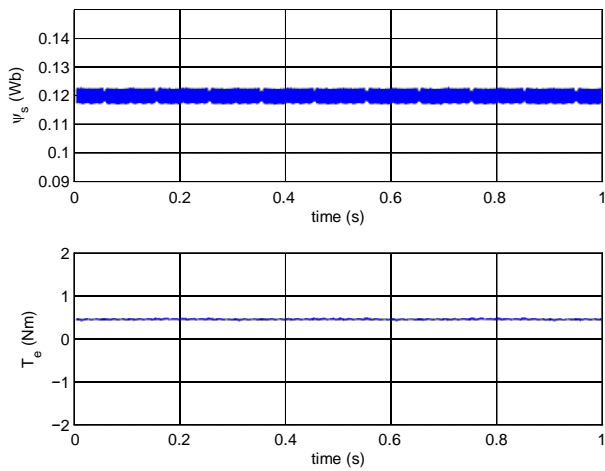Fig. 10.   Steady state response at 2000 rpm for DTC1

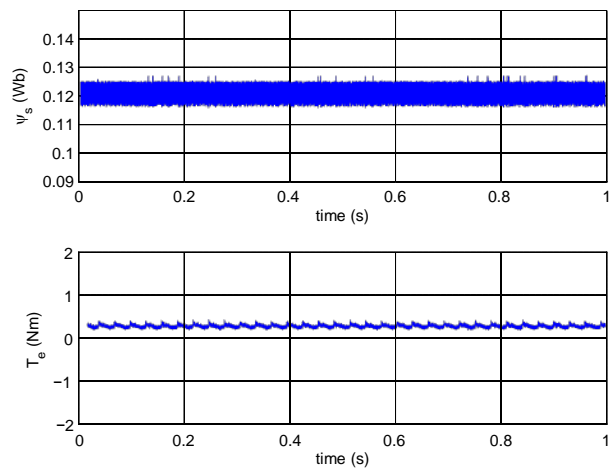Fig. 8.   Steady state response at 200 rpm for DTC2

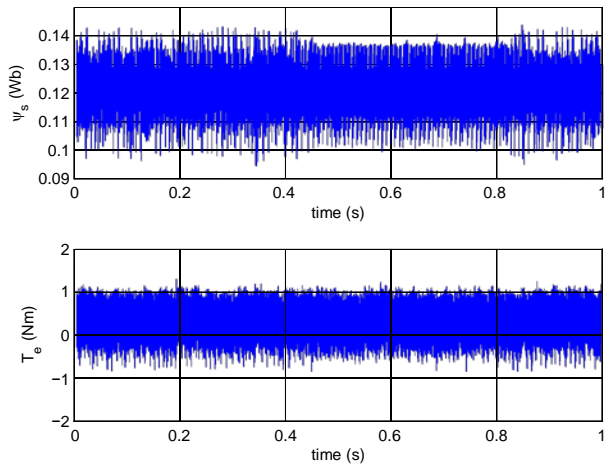Fig. 11.   Steady state response at 2000 rpm for DTC2

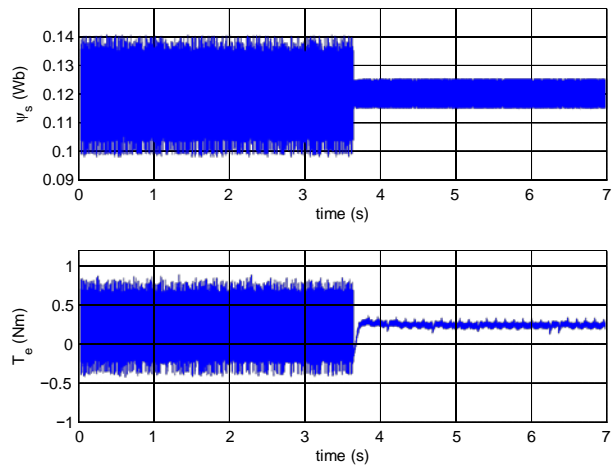Fig. 9.   Steady state response at 2000 rpm for classical DTC

Fig. 12.   Switching from DTC1 to DTC2 at 500 rpm (experimental)

The steady stator flux loci of motor at low speed and high speed for the three kinds of DTC are presented in Fig. 13, Fig. 14 and Fig. 15. Although the flux ripples of DTC1 are comparable to classical DTC, the stator flux loci of DTC1 are closer to circles than those in classical DTC. The stator flux loci of DTC2 are even better with good circle shape and small ripples. At low speed, the vector length should be small to achieve a smooth stator flux, so DTC2 presents better performance than DTC1 in Fig. 14 with fixed vector length.
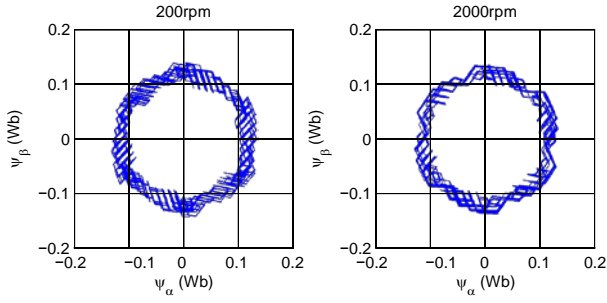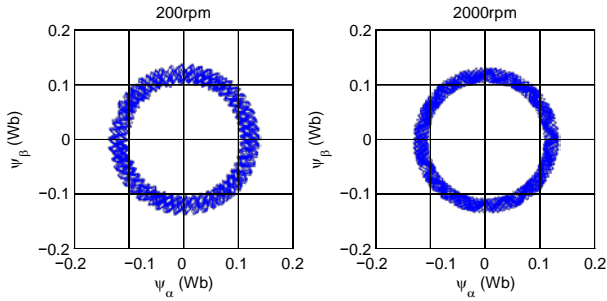
Fig. 13. Stator flux locus for classical DTC

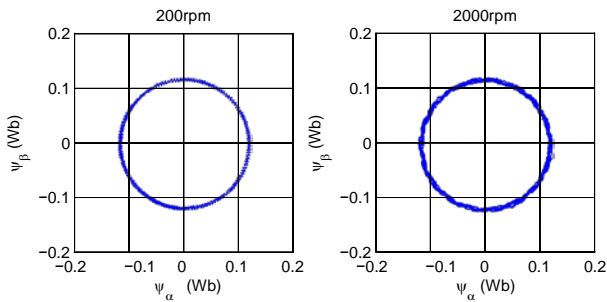Fig. 14. Stator flux locus for DTC1

Fig. 15. Stator flux locus for DTC2

are calculated as follows

$$T_{ripple} = \sqrt{\frac{1}{N} \sum_{i=1}^{N} (T_e(i) - T_{av})^2} \qquad (22)$$

$$\psi_{ripple} = \sqrt{\frac{1}{N} \sum_{i=1}^{N} (\psi_s(i) - \psi_{av})^2} \qquad (23)$$

where N represents the number of sampling points; T_{av} and ψ_{av} are the average value of torque and stator flux over N sampling points, respectively.
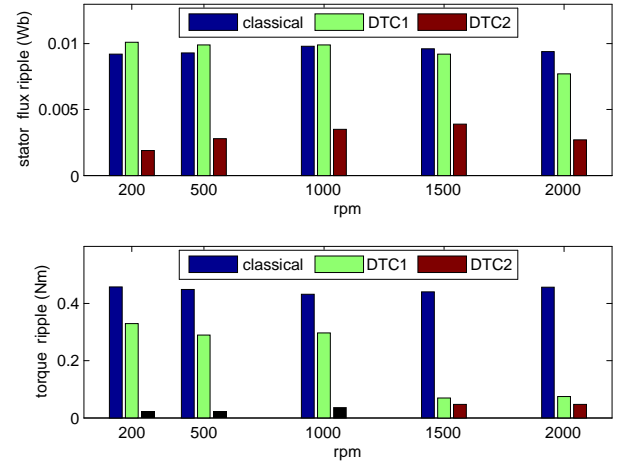

Fig. 16. Comparisons of torque and flux ripples for conventional DTC and proposed DTC (experimental)

Apart from the steady state tests, the dynamic response and robustness against disturbance are also carried out. Fig. 17, 18 and 19 show the start-up response without load from standstill to 2000 rpm for classical DTC, DTC1 and DTC2, respectively. By introducing anti-windup in the PI controller, the motor speed accelerates to the nominal speed quickly without overshoot. The dynamic response differences among classical DTC, DTC1 and DTC2 are insignificant, but the torque and flux ripples in DTC1 and DTC2 are reduced significantly, especially in DTC2.

The numerical comparisons of torque and flux ripples in conventional DTC and proposed DTC1 and DTC2 are illustrated in Fig. 16. There is an average ripple reduction of 92.4% for torque and 68.84% for flux in DTC2, validating the effectiveness of regulating both amplitude and length of voltage vectors. If only the angle of vector is regulated, it can be seen from Fig. 16 that the average flux ripple is slightly higher than that of classical DTC except at high speed. Nevertheless, there is still significant torque ripple reduction with an average value of 52.53%, about 28.03% at 200 rpm and 83.65% at 2000 rpm. The results under loaded condition are similar to that without load. The torque and flux ripples

The responses to external load disturbance of 2 Nm are illustrated in Fig. 20, 21 and 22 for conventional DTC, DTC1 and DTC2, respectively. DTC1 presents similar dynamic response to that of classical DTC. For DTC2, to enhance the dynamic performance and decrease the speed drop when external load is applied, the vector length calculation is disabled when the motor speed error falls out of a certain range of 50 rpm, as shown in Fig. 22. During the transient process, only the vector angle is regulated, so the dynamic response is similar to that in DTC1 shown in Fig. 21. The vector length calculation is re-enabled when the motor speed error is less than 50 rpm. This does not degrade the dynamic response while maintaining excellent performance in steady state.
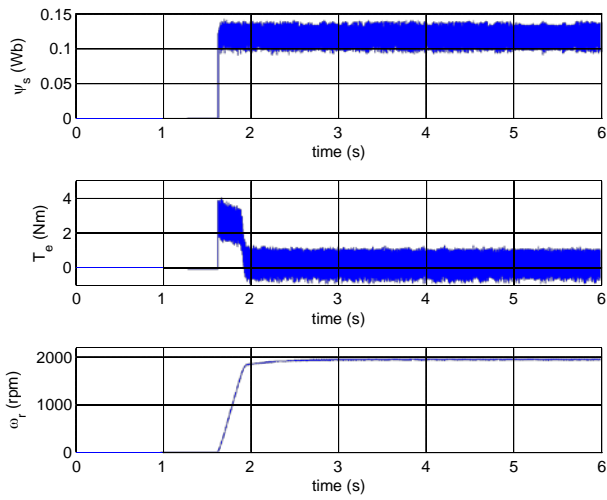
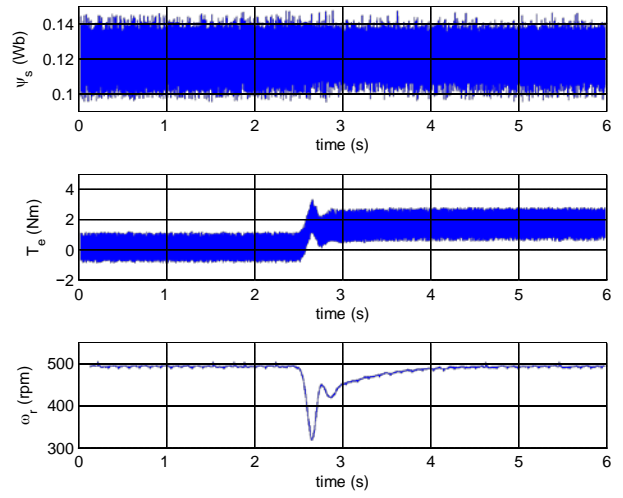Fig. 17. Start-up responses from 0 rpm to 2000 rpm for classical DTC

Fig. 18. Start-up responses from 0 rpm to 2000 rpm for DTC1

Fig. 19. Start-up responses from 0 rpm to 2000 rpm for DTC2

Fig. 20. Responses to external disturbance for classical DTC

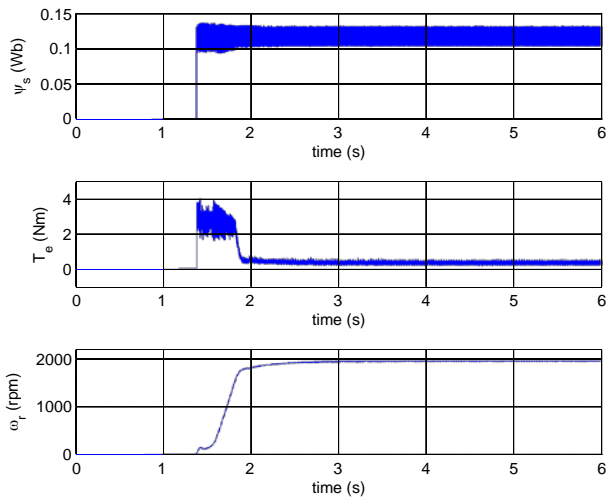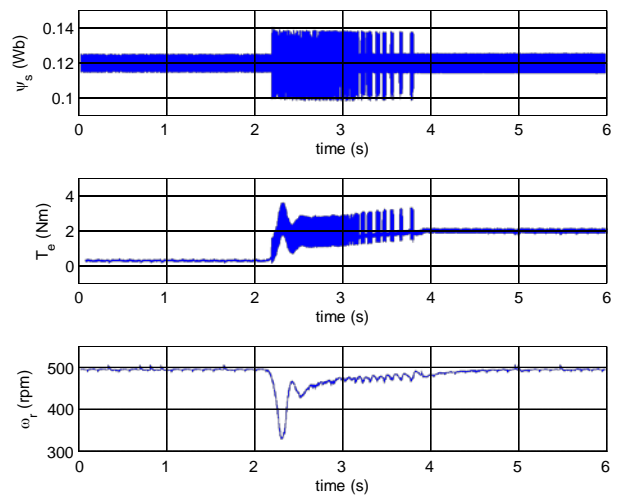Fig. 21. Responses to external disturbance for DTC1

Fig. 22. Responses to external disturbance for DTC2

VI. Conclusions

In this paper, a novel DTC is proposed to overcome the drawbacks of large torque ripple and variable switching frequency in classical switching-table-based DTC. Both the amplitude and phase of voltage vectors are regulated to control the torque and flux more accurately and moderately than the existing methods. The novel DTC employs SVM to achieve fixed switching frequency and reduced torque ripple. A simple method is developed to obtain the commanding voltage vector from the torque and flux errors only, and neither motor parameter or rotary coordinate transformation is needed. To further improve the performance of system, a LPF-based voltage model with appropriate compensation is employed to acquire the accurate information of stator flux. Extensive experimental results prove that the system can achieve excellent steady state performance and quick dynamic response while retaining the merits of simplicity and robustness as in classical DTC.

References

[1] M.-C. Chou and C.-M. Liaw, "Development of robust current 2-dof controllers for a permanent magnet synchronous motor drive with reaction wheel load," IEEE Trans. Power Electron., vol. 24, no. 5, pp. 1304 –1320, May 2009.

[2] B. Cheng and T. R. Tesch, "Torque feedforward control technique for permanent-magnet synchronous motors," IEEE Trans. Ind. Electron., vol. 57, no. 3, pp. 969 –974, Mar. 2010.

[3] G.-D. Andreescu, C. Pitic, F. Blaabjerg, and I. Boldea, "Combined flux observer with signal injection enhancement for wide speed range sensorless direct torque control of ipmsm drives," IEEE Trans. Energy Convers., vol. 23, no. 2, pp. 393–402, June 2008.

[4] J. Lee, J. Hong, K. Nam, R. Ortega, L. Praly, and A. Astolfi, "Sensorless control of surface-mount permanent-magnet synchronous motors based on a nonlinear observer," IEEE Trans. Power Electron., vol. 25, no. 2, pp. 290 –297, Feb. 2010.

[5] I. Boldea, M. Paicu, and G.-D. Andreescu, "Active flux concept for motion-sensorless unified ac drives," IEEE Trans. Power Electron., vol. 23, no. 5, pp. 2612–2618, Sept. 2008.

[6] I. Takahashi and T. Noguchi, "A new quick-response and high-efficiency control strategy of an induction motor," IEEE Trans. Ind. Appl., vol. IA-22, no. 5, pp. 820–827, Sept. 1986.

[7] M. Depenbrock, "Direct self-control (dsc) of inverter-fed induction machine," IEEE Trans. Power Electron., vol. 3, no. 4, pp. 420–429, Oct. 1988.

[8] G. S. Buja and M. P. Kazmierkowski, "Direct torque control of pwm inverter-fed ac motors - a survey," IEEE Trans. Ind. Electron., vol. 51, no. 4, pp. 744–757, Aug. 2004.

[9] R. M. H. W. L. K. Zhong, L., "Analysis of direct torque control in permanent magnet synchronous motor drives," IEEE Trans. Power Electron., vol. 12, no. 3, pp. 528 –536, May 1997.

[10] Z. Xu and M. Rahman, "Direct torque and flux regulation of an ipm synchronous motor drive using variable structure control approach," IEEE Trans. Power Electron., vol. 22, no. 6, pp. 2487 –2498, Nov. 2007.

[11] G. Foo and M. Rahman, "Sensorless direct torque and flux-controlled ipm synchronous motor drive at very low speed without signal injection," IEEE Trans. Ind. Electron., vol. 57, no. 1, pp. 395 –403, Jan. 2010.

[12] D. Casadei, F. Profumo, G. Serra, and A. Tani, "Foc and dtc: two viable schemes for induction motors torque control," IEEE Trans. Power Electron., vol. 17, no. 5, pp. 779–787, Sep. 2002.

[13] Y. Zhang, Z. Zhao, J. Zhu, W. Xu, and D. G. Dorrell, "Speed sensorless direct torque control of 3-level inverter-fed induction motor drive based on optimized switching table," in Proc. the 35th Annual Conference of the IEEE Industrial Electronics Society, IECON '09., 2009, pp. 1318–1323.

[14] X. del Toro Garcia, A. Arias, M. Jayne, and P. Witting, "Direct torque control of induction motors utilizing three-level voltage source inverters," IEEE Trans. Ind. Electron., vol. 55, no. 2, pp. 956–958, Feb. 2008.

[15] T. Geyer, G. Papafotiou, and M. Morari, "Model predictive direct torque controlpart i: Concept, algorithm, and analysis," IEEE Trans. Ind. Electron., vol. 56, no. 6, pp. 1894–1905, Jun. 2009.

[16] H. Miranda, P. Cortes, J. I. Yuz, and J. Rodriguez, "Predictive torque control of induction machines based on state-space models," IEEE Trans. Ind. Electron., vol. 56, no. 6, pp. 1916–1924, Jun. 2009.

[17] N. West and R. Lorenz, "Digital implementation of stator and rotor flux-linkage observers and a stator-current observer for deadbeat direct torque control of induction machines," IEEE Trans. Ind. Appl., vol. 45, no. 2, pp. 729–736, Mar./Apr. 2009.

[18] Y. Zhang, J. Zhu, Y. Guo, W. Xu, Y. Wang, and Z. Zhao, "A sensorless dtc strategy of induction motor fed by three-level inverter based on discrete space vector modulation," in Proc. Australasian Universities Power Engineering Conference AUPEC 2009, Sep. 27–30, 2009, pp. 1–6.

[19] Y. Zhang, Z. Zhao, T. Lu, and L. Yuan, "Sensorless 3-level inverter-fed induction motor drive based on indirect torque control," in Proc. IEEE 6th International Power Electronics and Motion Control Conference IPEMC '09, May 17–20, 2009, pp. 589–593.

[20] J. Beerten, J. Verveckken, and J. Driesen, "Predictive direct torque control for flux and torque ripple reduction," IEEE Trans. Ind. Electron., vol. 57, no. 1, pp. 404–412, Jan. 2010.

[21] E. Flach, R. Hoffmann, and P. Mutschler, "Direct mean torque control of an induction motor," in Proc. EPE, vol. 3, 1997, pp. 672–677.

[22] D. Casadei, G. Serra, and A. Tani, "Improvement of direct torque control performance by using a discrete svm technique," in Proc. PESC 98 Record Power Electronics Specialists Conference 29th Annual IEEE, vol. 2, May 17–22, 1998, pp. 997–1003.

[23] J.-K. Kang and S.-K. Sul, "New direct torque control of induction motor for minimum torque ripple and constant switching frequency," IEEE Trans. Ind. Appl., vol. 35, no. 5, pp. 1076–1082, Sep./Oct. 1999.

[24] L. Romeral, A. Arias, E. Aldabas, and M. Jayne, "Novel direct torque control (dtc) scheme with fuzzy adaptive torque-ripple reduction," IEEE Trans. Ind. Electron., vol. 50, no. 3, pp. 487–492, June 2003.

[25] G. Abad, M. A. Rodriguez, and J. Poza, "Two-level vsc based predictive direct torque control of the doubly fed induction machine with reduced torque and flux ripples at low constant switching frequency," IEEE Trans. Power Electron., vol. 23, no. 3, pp. 1050–1061, May 2008.

[26] K.-B. Lee, J.-H. Song, I. Choy, and J.-Y. Yoo, "Torque ripple reduction in dtc of induction motor driven by three-level inverter with low switching frequency," IEEE Trans. Power Electron., vol. 17, no. 2, pp. 255–264, Mar. 2002.

[27] H. Hu and Y. Li, "Predictive direct torque control strategies of induction motor based on area voltage vectors table," in Proc. the 29th Annual Conference of the IEEE Industrial Electronics Society, IECON '03, vol. 3, Nov. 2003, pp. 2684 – 2689.

[28] C. Lascu and A. Trzynadlowski, "Combining the principles of sliding mode, direct torque control, and space-vector modulation in a high- performance sensorless ac drive," IEEE Trans. Ind. Appl., vol. 40, no. 1, pp. 170–177, Jan./Feb. 2004.

[29] Y.-S. Lai and J.-H. Chen, "A new approach to direct torque control of induction motor drives for constant inverter switching frequency and torque ripple reduction," IEEE Trans. Energy Convers., vol. 16, no. 3, pp. 220–227, Sep 2001.

[30] V. Ambrozic, G. S. Buja, and R. Menis, "Band-constrained technique for direct torque control of induction motor," IEEE Trans. Ind. Electron., vol. 51, no. 4, pp. 776–784, Aug. 2004.

[31] B. Kenny and R. Lorenz, "Stator- and rotor-flux-based deadbeat direct torque control of induction machines," IEEE Trans. Ind. Appl., vol. 39, no. 4, pp. 1093–1101, July/Aug. 2003.

[32] L. Tang, L. Zhong, M. Rahman, and Y. Hu, "A novel direct torque controlled interior permanent magnet synchronous machine drive with low ripple in flux and torque and fixed switching frequency," IEEE Trans. Power Electron., vol. 19, no. 2, pp. 346–354, Mar. 2004.

[33] S. Kouro, R. Bernal, H. Miranda, C. Silva, and J. Rodriguez, "High-performance torque and flux control for multilevel inverter fed induction motors," IEEE Trans. Power Electron., vol. 22, no. 6, pp. 2116–2123, Nov. 2007.

[34] S. Kouro, P. Cortes, R. Vargas, U. Ammann, and J. Rodriguez, "Model predictive control—a simple and powerful method to control power converters," IEEE Trans. Ind. Electron., vol. 56, no. 6, pp. 1826 –1838, Jun. 2009.

[35] M.-H. Shin, D.-S. Hyun, S.-B. Cho, and S.-Y. Choe, "An improved stator flux estimation for speed sensorless stator flux orientation control of induction motors," IEEE Trans. Power Electron., vol. 15, no. 2, pp. 312–318, Mar. 2000.